J. Fluid Mech. (2007), *vol.* 586, *pp.* 323–345. © 2007 Cambridge University Press
doi:10.1017/S0022112007007057 Printed in the United Kingdom

Long-wave-induced flows in an unsaturated permeable seabed

PHILIP L.-F. LIU, YONG SUNG PARK AND JAVIER L. LARA

School of Civil and Environmental Engineering, Cornell University, Ithaca, NY 14853, USA

(Received 19 December 2006 and in revised form 20 April 2007)

We present both analytical and numerical solutions describing seepage flows in an unsaturated permeable seabed induced by transient long waves. The effects of compressibility of pore water in the seabed due to a small degree of unsaturation are considered in the investigation. To make the problem tractable analytically, we first focus our attention on situations where the horizontal scale of the seepage flow is much larger than the vertical scale. With this simplification the pore-water pressure in the soil column is governed by a one-dimensional diffusion equation with a specified pressure at the water–seabed interface and the no-flux condition at the bottom of the seabed. Analytical solutions for pore-water pressure and velocity are obtained for arbitrary transient waves. Special cases are studied for periodic waves, cnoidal waves, solitary waves and bores. Numerical solutions are also obtained by simultaneously solving the Navier–Stokes equations for water wave motions and the exact two-dimensional diffusion equation for seepage flows in the seabed. The analytical solutions are used to check the accuracy of the numerical methods. On the other hand, numerical solutions extend the applicability of the analytical solutions. The liquefaction potential in a permeable bed as well as the energy dissipation under various wave conditions are then discussed.

1. Introduction

In shallow water, wind waves interact with the seabed, resulting in a number of phenomena. Bathymetric variations affect the direction of wave propagation and the spatial variation of wave heights, commonly known as refraction and diffraction. The wave–seabed interaction also leads to energy dissipation. Over a rigid seabed, shear flows in a laminar or turbulent boundary layer contribute to wave attenuation over a distance of many wavelengths. If the seabed is composed of sediments, a variety of dissipation mechanisms associated with the sediment rheology play different roles in enhancing wave damping and modifying wave characteristics. For instance, the effects of percolation might become important if seabed sediments consist of coarse sand or shingle. With fine sediment grain sizes, the sea bottom becomes deformable under wave loading and the effects of poro-elasticity need to be considered in estimating energy dissipation. When the seabed consists of silt or mud, the physical processes become more complex. Depending on the density of the mud, it may behave like a viscous fluid, or visco-elastic materials or visco-plastic materials.

Within the framework of linear wave theory, theoretical formulae for the wave attenuation rate and the modified dispersion relationship of simple harmonic progressive waves are available if the seabed properties and rheology can be specified *a priori* (e.g. Liu 1973; Dalrymple & Liu 1978; Yamamoto *et al.* 1978; MacPherson

https://doi.org/10.1017/S0022112007007057 Published online by Cambridge University Press

1980; Wen & Liu 1998; Liu & Chan 2007*a*). In shallow water, waves are usually nonlinear and possibly dispersive. Linear wave theory is no longer adequate. In recent years, Boussinesq-type models have been extensively developed as practical phase-resolving wave models in both intermediate and shallow water (i.e. from the continental shelf to the surf zone). The phase-resolving nature of the Boussinesq-type models is essential in better understanding and predicting nearshore processes (Mei & Liu 1993). Therefore, transient wave-induced flows inside a seabed require further attention.

In their study of the interaction of long waves and a viscous fluid mud bed, Liu & Chan (2007*b*) presented a new set of Boussinesq equations. Using these equations they provided the analytical solutions for solitary wave damping. In this paper, we shall focus our attention on the seepage flows inside a sandy seabed, induced by arbitrary long waves. Furthermore, we shall consider the situation where some air bubbles have been trapped in the seabed so that the compressibility of the fluid mixture is not negligible. Earlier investigations have only concentrated either on the small-amplitude periodic waves (e.g. Moshagen & Torum 1975) or on fully saturated porous media flows (e.g. Packwood & Peregrine 1980). Because of the low permeability, the effects of a sandy seabed on wave motions are usually weak. Therefore, the seepage flow characteristics can be analysed by assuming that the waves have not been affected by the presence of the permeable seabed. Once the seepage flow solutions are obtained, the energy dissipation can be estimated by calculating the pressure work done along the water–seabed interface, which can become significant when waves propagate a long distance. The seepage flow solutions can also be used to assess the liquefaction potential in the seabed (Madsen 1974; Packwood & Peregrine 1980; Sumer & Fredsoe 2002; Jeng 2003).

The paper is organized in the following manner. We will first present a general analytical solution for the seepage flows in a thin layer of seabed, induced by arbitrary transient long waves. Based on this analytical solution, pore-water pressure and seepage velocities under periodic waves, cnoidal waves, solitary waves and bores are examined. To ensure the correctness and the limitations of the analytical solutions, direct numerical solutions (DNS) for fully coupled wave motions and seepage flows in the seabed are also obtained by solving the Navier–Stokes equations in the flow field above the seabed and Darcy's flow equation in the seabed. On one hand, the DNS results are compared with the analytical solutions to validate the accuracy of the numerical scheme. On the other hand, the soundness and the limitations of the approximations employed in the analytical solutions are further examined with the DNS solutions. In the discussion section, the liquefaction potential inside the seabed under various wave conditions is discussed. The energy dissipation and wave damping rate are also examined for solitary waves.

2. Formulation

We consider a train of periodic waves or transient waves propagating over a permeable seabed with a thickness of d'. In the seabed seepage flows are generated by the dynamic pressure along the water–seabed interface. Darcy's law can be used to describe the seepage flow velocity (Bear 1972):

$$u' = -\frac{k'}{\rho' g'}\frac{\partial p'}{\partial x'}, \quad w' = -\frac{k'}{\rho' g'}\frac{\partial p'}{\partial z'}, \tag{2.1}$$

https://doi.org/10.1017/S0022112007007057 Published online by Cambridge University Press

where (u', w') denotes the horizontal (x') and the vertical (z') components of the seepage velocity, p' the pore-water pressure, k' the hydraulic conductivity of the porous bed, ρ' the density of the fluid, and g' the gravitational acceleration. Substituting the above equations into that for the conservation of mass shows that the pore-water pressure satisfies the following diffusion equation (Bear 1972):

$$\frac{k'}{\rho' g'}\left(\frac{\partial^2 p'}{\partial x'^2}+\frac{\partial^2 p'}{\partial z'^2}\right)=\frac{n}{\overline{K}'_w}\frac{\partial p'}{\partial t'}, \tag{2.2}$$

in which t' is the time and n the porosity. $\overline{K}'_w$ is the effective bulk modulus of elasticity of the fluid taking ino account gas (air) in the fluid, i.e.

$$\frac{1}{\overline{K}'_w}=\frac{1}{K'_w}+\frac{1-S_r}{p'_{abs}}, \tag{2.3}$$

where K'_w is the bulk modulus of elasticity of the pure water, S_r the degree of saturation, and p'_{abs} ($100\,\mathrm{kN\,m^{-2}}$) the absolute pore-water pressure. For pure water, K'_w is $2.3\times10^9\,\mathrm{N\,m^{-2}}$. With a small fraction of gas in the water, say $S_r=0.995$, the effective bulk modulus of elasticity decreases by almost two orders of magnitude, i.e. $\overline{K}'_w=2\times10^7\,\mathrm{N\,m^{-2}}$.

Denoting the horizontal and vertical length scales for the flow motions in the seabed as L'_x and L'_z, respectively, and the time scale as T', the dimensionless governing equation for the seepage flows can be expressed as:

$$D_x\frac{\partial^2 p}{\partial x^2}+D_z\frac{\partial^2 p}{\partial z^2}=\frac{\partial p}{\partial t}, \tag{2.4}$$

in which the variables without primes are dimensionless and the dimensionless parameters D_x and D_z are

$$D_x=\frac{k'\overline{K}'_w}{\rho' g' n}\frac{T'}{L'^2_x},\quad D_z=D_x\left(\frac{L'_x}{L'_z}\right)^2. \tag{2.5}$$

The pressure field has been normalized by $p'_0=\rho' g' a'$, where a' characterizes the wave amplitude. Along the water–seabed interface, the pressure is continuous:

$$p=p_b(x,t)\quad\text{at } z=0, \tag{2.6}$$

where p_b is the dimensionless dynamic pressure at the seabed associated with the transient wave propagating above the seabed. Along the rock bottom of the seabed, $z=-d$, the no-flux condition is applied

$$\frac{\partial p}{\partial z}=0\quad\text{at } z=-d. \tag{2.7}$$

With proper specification of initial condition for the pressure field in the seabed and two lateral (x-direction) boundary conditions, the initial-boundary-value problem can be solved. For an arbitrary pressure distribution along the water–seabed interface, $p_b(x,t)$, an analytical solution is not obtainable. However, a numerical solution is always possible.

It is clear from (2.1) that the seepage velocity scales are $k'a'/L'_x$ and $k'a'/L'_z$ in the horizontal and vertical directions, respectively. Since the hydraulic conductivity is usually quite small, e.g. $k'=10^{-6}\,\mathrm{m\,s^{-1}}$ for coarse silt and $k'=10^{-4}\,\mathrm{m\,s^{-1}}$ for fine sand, the influence of the seepage flows on wave motions above the seabed is rather weak. One can first calculate the wave motions above the seabed by assuming that the

https://doi.org/10.1017/S0022112007007057 Published online by Cambridge University Press

seabed is impermeable. The dynamic pressure along the water–seabed interface can be found from the wave motion solutions. Once the seepage flow solutions are obtained, the wave damping rate caused by percolation can be estimated by calculating the energy dissipation in the seepage flow. However, if the full interaction between the wave motions and the seepage flows is desirable (i.e. the hydraulic conductivity is very large) the continuity of the velocity across the water–seabed interface are required and the flow motions above and inside the seabed must be solved simultaneously.

In the following section, we shall investigate a subset of the physical problems described by (2.4), for which we can derive analytical solutions. The fully coupled flow problem will then be discussed in § 4 by means of DNS.

3. Analytical solutions inside the permeable seabed

Since the seepage flows inside the seabed are induced by either transient or periodic long waves, it is reasonable to choose the characteristic wavelength as the horizontal length scale. From (2.5), it is obvious that if

$$O(L_z') \ll O(L_x'), \quad \text{then} \quad O(D_x) \ll O(D_z) \tag{3.1}$$

and the governing equation, (2.4), can be simplified to the one-dimensional diffusion equation. Hence,

$$D_z \frac{\partial^2 p}{\partial z^2} = \frac{\partial p}{\partial t}. \tag{3.2}$$

There are two possible choices for the vertical length scale: either the thickness of the seabed, d', or the vertical diffusion depth corresponding to the time scale of a transient wave event, T'. The latter can be defined by employing (2.5) as

$$L_z' = \left(\frac{k' \overline{K}_w' T'}{\rho' g' n} \right)^{1/2}. \tag{3.3}$$

We reiterate here that for a transient wave event, such as a solitary wave, the time scale, T', is effectively finite and the diffusion depth, (3.3), can be either larger or smaller than the thickness of the porous bed. On the other hand, in the case of periodic wave loading, if the quasi-steady state is reached, the vertical length scale is determined by the thickness of the bed.

Introducing a stretched vertical coordinate,

$$\eta = \frac{z}{\sqrt{D_z}}, \tag{3.4}$$

the simplified governing equation, (3.2), becomes

$$\frac{\partial^2 p}{\partial \eta^2} = \frac{\partial p}{\partial t}. \tag{3.5}$$

From (2.6) the boundary condition along the water–seabed interface can be rewritten as

$$p = p_b(x, t) \quad \text{at } \eta = 0. \tag{3.6}$$

Along the rock bottom of the seabed, $\eta = -\overline{d} = -d/\sqrt{D_z}$, the no-flux condition, (2.7), takes the following form:

$$\frac{\partial p}{\partial \eta} = 0 \quad \text{at } \eta = -\overline{d}. \tag{3.7}$$

https://doi.org/10.1017/S0022112007007057 Published online by Cambridge University Press

Finally, in the following analysis we will assume that the dynamic pressure inside the seabed is zero initially.

The analytical solution for the two-point initial-boundary-value problem, (3.5), (3.6), and (3.7), can be obtained by superimposing the fundamental solution for the diffusion equation and using the method of images to satisfy the boundary conditions. Thus,

$$p(x,\eta,t) = \int_0^t \frac{\partial p_b}{\partial \tau}\operatorname{erfc}\left[\frac{-\eta}{\sqrt{4(t-\tau)}}\right]\mathrm{d}\tau + \sum_{\mathrm{n}=1}^{\infty}(-1)^{\mathrm{n}}\int_0^{\mathrm{t}}\frac{\partial p_b}{\partial \tau}\left\{-\operatorname{erfc}\left[\frac{\eta+2n\bar{d}}{\sqrt{4(t-\tau)}}\right]+\operatorname{erfc}\left[\frac{-\eta+2n\bar{d}}{\sqrt{4(t-\tau)}}\right]\right\}\mathrm{d}\tau. \quad (3.8)$$

The non-dimensional velocities can be obtained by differentiating the pressure given in (3.8):

$$u = -\frac{\partial p}{\partial x} = -\int_0^t \frac{\partial^2 p_b}{\partial \tau\,\partial x}\operatorname{erfc}\left[\frac{-\eta}{\sqrt{4(t-\tau)}}\right]\mathrm{d}\tau - \sum_{n=1}^{\infty}(-1)^n\int_0^t\frac{\partial^2 p_b}{\partial \tau\,\partial x}\left\{-\operatorname{erfc}\left[\frac{\eta+2n\bar{d}}{\sqrt{4(t-\tau)}}\right]+\operatorname{erfc}\left[\frac{-\eta+2n\bar{d}}{\sqrt{4(t-\tau)}}\right]\right\}\mathrm{d}\tau, \quad (3.9)$$

and

$$w = -\frac{1}{\sqrt{D_z}}\frac{\partial p}{\partial \eta} = -\frac{1}{\sqrt{\pi D_z}}\left\{\int_0^t \frac{\partial p_b}{\partial \tau}\frac{1}{\sqrt{t-\tau}}\exp\left[-\frac{\eta^2}{4(t-\tau)}\right]\mathrm{d}\tau + \sum_{n=1}^{\infty}(-1)^n\int_0^t\frac{\partial p_b}{\partial \tau}\frac{1}{\sqrt{t-\tau}}\left(\exp\left[-\frac{(\eta+2n\bar{d})^2}{4(t-\tau)}\right]+\exp\left[-\frac{(\eta-2n\bar{d})^2}{4(t-\tau)}\right]\right)\mathrm{d}\tau\right\}. \quad (3.10)$$

If the pressure at the water–seabed interface, p_b, is specified, we can describe the temporal and spatial variations of the pressure and velocity components inside the seabed using (3.8), (3.9), and (3.10).

3.1. *Comparisons between experimental data and theoretical solutions*

In this section, we compare the analytical solutions for the pore-water pressure field under a sinusoidal wavetrain with the experimental data reported by Oumeraci & Kudella (2004). In the experiments, sinusoidal waves of wave height $H' = 2a' = 0.6\,\mathrm{m}$ and wave period $T' = 4.5\,\mathrm{s}$ propagate in a water depth of 1.6 m. Using the linear wave theory, the corresponding wavelength is $L'_x = 16.88\,\mathrm{m}$. The seabed is made of medium/fine sand with $D'_{50} = 0.21\,\mathrm{mm}$ and a total thickness $d' = 2.45\,\mathrm{m}$. The following soil properties are measured: porosity $n = 0.45$ and hydraulic conductivity $k' = 10^{-4}\,\mathrm{m\,s^{-1}}$. We note that the degree of saturation is not directly measured in the experiments. Using the measured values for physical variables and estimated value of $S_r = 0.990$, the dimensionless parameters can be readily obtained:

$$\frac{L'_z}{L'_x} = 0.1451, \quad D_x = 3.6\times10^{-3}, \quad D_z = 0.169.$$

Expressing the dynamic pressure at the water–seabed interface, p_b, under a sinusoidal wavetrain as

$$p_b = \mathrm{Re}\,\{\exp[\mathrm{i}2\pi(x-t)]\}, \quad (3.11)$$

https://doi.org/10.1017/S0022112007007057 Published online by Cambridge University Press

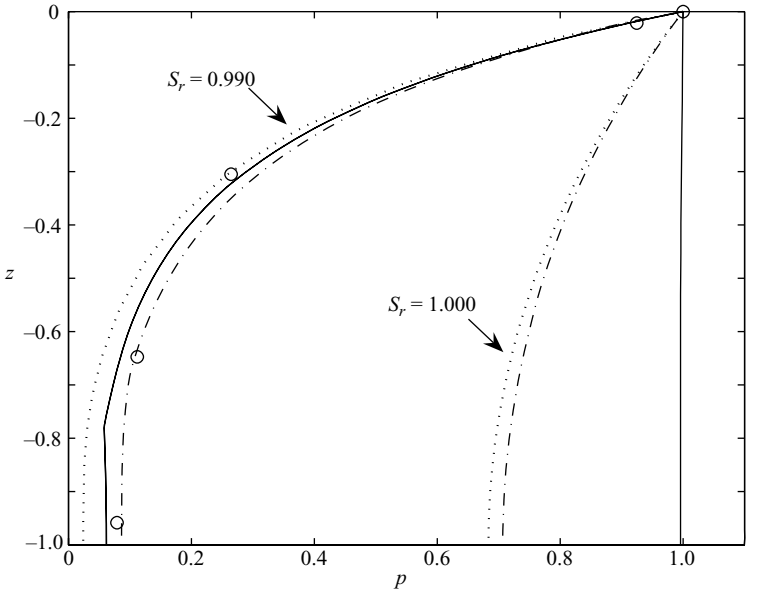


FIGURE 1. Comparison of maximum pore-water pressure amplitudes for $S_r = 0.990$ and 1.000: ·····, two-dimensional analytical solutions (3.12); ——, one-dimensional analytical solutions (3.8); —•—, two-dimensional DNS solutions; ○, the experimental data (Oumeraci & Kudella 2004).

the quasi-steady pressure field inside the porous bed can be analytically obtained as (e.g. Moshagen & Torum 1975)

$$p = \mathrm{Re}\left\{\frac{1}{\cosh\lambda\overline{d}}\cosh\lambda(\eta+\overline{d})\exp\left[\mathrm{i}2\pi(x-t)\right]\right\}, \tag{3.12}$$

in which λ is a complex constant with modulus

$$|\lambda| = \sqrt{2\pi}[(2\pi D_x)^2+1]^{1/4}, \tag{3.13}$$

and argument

$$\mathrm{Arg}(\lambda) = \frac{1}{2}\arctan\left(\frac{1}{2\pi D_x}\right). \tag{3.14}$$

We remark here that if the approximation in (3.1) is applicable, D_x can be considered negligible in (3.13) and (3.14). Thus, $\lambda = (1-\mathrm{i})\sqrt{\pi}$. On the other hand, if the seabed is saturated, $\overline{K}'_w$ becomes much greater than one. The governing equation, (2.2), can be reduced to the Laplace equation. Therefore, in the dimensional form the pore-water pressure is no longer a function of the elasticity of the water and decays into the seabed with the scale of wavelength (e.g. Liu 1973). Hence, λ can be approximated as a real number: $\lambda = 2\pi\sqrt{D_x}$.

Since the value of D_x is not very large in the experiments and the thickness of the seabed is much smaller than the wavelength, the assumptions made in the theoretical solutions, (3.8), are satisfied. We anticipate a good agreement between the experimental data and theoretical results. Oumeraci & Kudella (2004) provided experimental data for the maximum pore-water pressure amplitude profile under the sinusoidal wavetrain and their data are shown in figure 1. The integrals in equation (3.8) are evaluated using Matlab's 'quad' function, which approximates the integral of a

https://doi.org/10.1017/S0022112007007057 Published online by Cambridge University Press

function to within an error of 10^{-6} using recursive adaptive Simpson quadrature. Twenty terms in the series are used, although the solution has already converged when ten terms are used. In the same figure, we also show the theoretical results based on (3.12) for both saturated and unsaturated conditions. It is clear that the pressure response is sensitive to the degree of saturation. Oumeraci & Kudella (2004) did not directly measure the degree of saturation in their experiments. Based on the comparisons shown in figure 1, we speculate that the degree of saturation is about 0.990. We also remark here that the current theoretical solution is a transient solution where the pressure field begins from a quiescent state. Therefore, the order-of-magnitude estimation for the time to establish the 'quasi-steady state' in the seabed can be obtained from (3.3) by assigning the thickness of the seabed, d', as the vertical length scale, L'_z. Thus, for the experiments, the diffusion time scale, with $S_r = 0.990$, to reach quasi-steady state is about 27 s, which corresponds to six wave periods. The diffusion time scale becomes shorter for a higher degree of saturation, e.g. 2.8 s for $S_r = 0.999$. In the same figure the DNS results, which will be discussed in a later section, are also shown. The numerical solutions and two analytical solutions agree reasonably well with the experimental data. The approximate analytical solution fails for the saturated condition.

3.2. *Examples*

In this section, we show various features of the pressure field and the velocity field inside a seabed under different wave loadings, including sinusoidal wave, cnoidal wave, solitary wave and bore, obtained by assigning $D_z = 1$ and $d = 1$.

3.2.1. *Sinusoidal wave*

The analytical solutions for the pressure field induced by a sinusoidal wavetrain have been presented for a specific experiment in the previous section. Here we provide a general and broader discussion. In figure 2 the time histories of pressure and velocity components at $x = 0$ are plotted at three different elevations, $\eta = 0, -0.5, -1.0$, respectively. Since (3.8) is derived from an initially quiescent state, with the chosen parameters ($D_z = 1$ and $d = 1$) it takes a couple of wave periods to establish the 'quasi-steady state', when the vertical diffusion length scale is the same as the thickness of the seabed. Note that initially the constant reference pressure is unity so that the velocity components are zero initially. The phase lags between the pressure and velocity responses at different elevations are apparent. The vertical pressure profiles at $x = 0$ and at four phases during the third wave period, calculated from the periodic solution (3.12) and the transient solution (3.8), are compared in figure 3(*b*). Also plotted are vertical profiles of x- and z-velocity components (figures 3*c* and 3*d*), where the periodic solutions are obtained by differentiating (3.12). The present approximate solutions are almost identical to the two-dimensional analytical solution, suggesting that the approximations employed in the present theory are satisfied.

Under the wave crest, the dynamic pressure reaches the maximum value at the water–seabed interface and decays quickly into the seabed, resulting in a downward (negative) seepage velocity. As the wave crest passes the observation point, $x = 0$, the dynamic pressure decreases on the interface. However, the dynamic pressure increases near the bottom of the seabed. Consequently, upward (positive) seepage velocities are developed. As the wave trough approaches the observation point, the dynamic pressure becomes negative in the seabed with upward seepage velocities in the entire seabed column. The implications of the upward seepage velocity on the seabed stability will be discussed later. As the wave crest approaches, the dynamic

https://doi.org/10.1017/S0022112007007057 Published online by Cambridge University Press

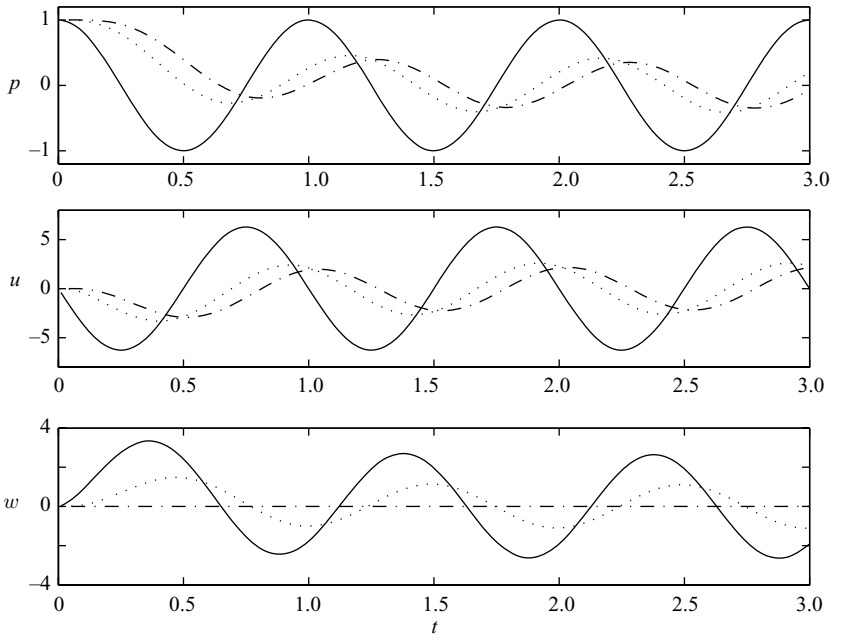


FIGURE 2. Time histories of dimensionless dynamic pressure, p, dimensionless horizontal seepage velocity, u, and dimensionless vertical seepage velocity, w, in a seabed under a periodic wavetrain at three different vertical locations inside the seabed: ——, $\eta = 0$; · · · · ·, $\eta = -0.5$; —·—, $\eta = -1.0$.

pressure in the seabed becomes positive with a downward seepage velocity again. Finally, we remark here that the vertical profiles of the dynamic pressure and the velocity components are symmetric with respect to the wave crest and the wave trough.

3.2.2. *Cnoidal wave*

The cnoidal wave can be defined by two dimensionless parameters: the nonlinearity $\epsilon = a'/h'$, and the modulus of the elliptic integral m, where $0 < m < 1$. Denoting the complete elliptic integrals of the first and second kinds with modulus m as K and E, respectively, the dimensionless dynamic pressure along the water–seabed interface, p_b, can be expressed as (Mei 1983)

$$p_b = \frac{K}{K-E}\left[\left(1 - m - \frac{E}{K}\right) + m\mathrm{Cn}^2(2K\xi)\right], \tag{3.15}$$

where Cn is the Jacobi elliptic function,

$$\xi = x - Ct \tag{3.16}$$

and the dimensionless wave speed is

$$C = \left[1 + \frac{\epsilon K}{K-E}\left(-m + 2 - \frac{3E}{K}\right)\right]^{1/2}. \tag{3.17}$$

https://doi.org/10.1017/S0022112007007057 Published online by Cambridge University Press

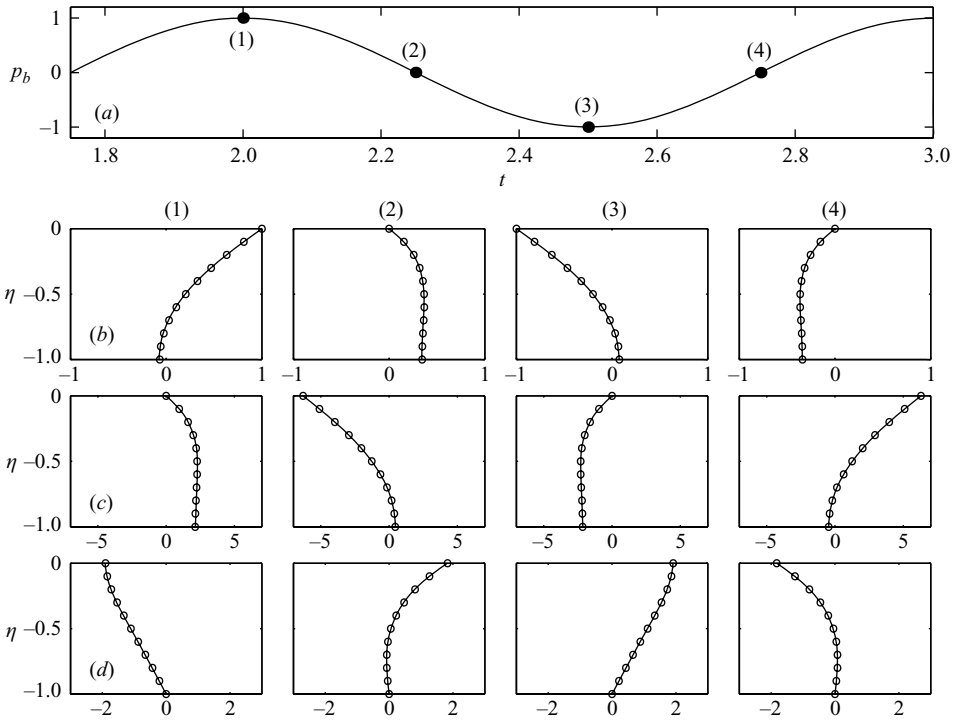


FIGURE 3. Vertical profiles of dimensionless dynamic pressure, p (b), dimensionless horizontal seepage velocity, u (c), and dimensionless vertical seepage velocity, w (d), in a seabed under a periodic wavetrain: ——, two-dimensional analytical solutions (3.12); ○, numerical integrations of (3.8). (a) The time history of the dimensionless dynamic pressure at the water–seabed interface, p_b. The vertical profiles are plotted at four different phases as indicated by numbers in brackets, corresponding to four columns.

Note that the wavelength has been used as the characteristic length scale, L'_x, which is given by

$$\frac{L'_x}{h'} = 4K\left(\frac{K-E}{3\epsilon K}\right)^{1/2}. \tag{3.18}$$

Cnoidal waves reduce to sinusoidal waves as m approaches zero, while as m goes to 1, they become a series of solitary waves. However, these two parameters ϵ and m are not entirely independent, that is, for a given m, there is a maximum possible value of ϵ which allows C in (3.17) to exist.

To evaluate the dynamic pressure inside the seabed, we need to differentiate (3.15) with respect to t:

$$\frac{\partial p_b}{\partial t} = \frac{4mCK^2}{K-E}\mathrm{Cn}(2K\xi)\mathrm{Sn}(2K\xi)\mathrm{Dn}(2K\xi), \tag{3.19}$$

where Cn, Sn, and Dn are Jacobi elliptic functions. As an example, solutions are obtained for the dimensionless dynamic pressure and velocity field corresponding to $\epsilon = 0.2$ and $m = 0.9$ In figure 4, time histories of pressures and velocities at $x = 0$ and at three elevations are shown. These solutions have already converged to the quasi-steady-state solutions at the end of the first period, as in the case of sinusoidal waves. Again, the upward (positive) seepage velocities exist and occur during different time intervals depending on the elevations.

https://doi.org/10.1017/S0022112007007057 Published online by Cambridge University Press

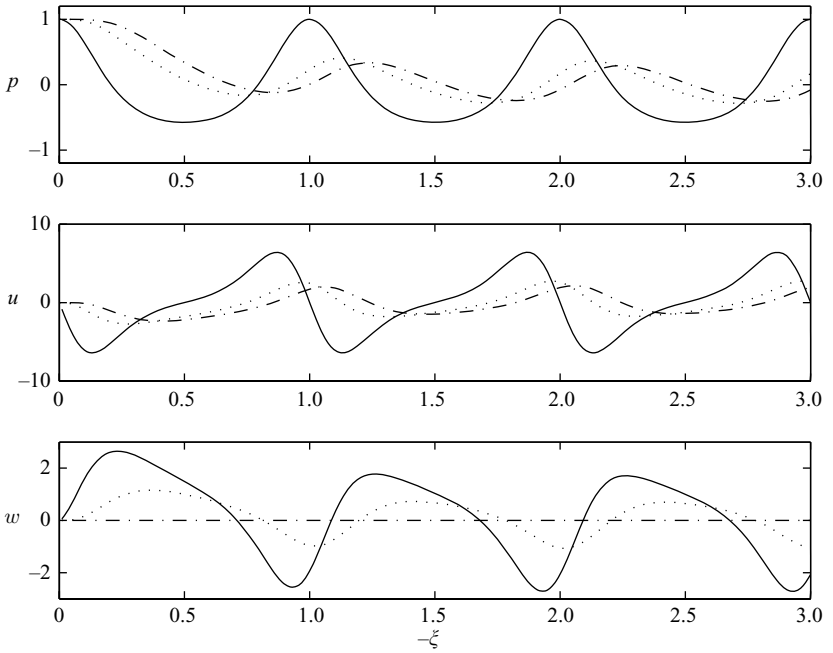


FIGURE 4. Time histories of dimensionless dynamic pressure, p, dimensionless horizontal seepage velocity, u, and dimensionless vertical seepage velocity, w, in a seabed under a cnoidal wavetrain at three different vertical locations inside the seabed: ——, $\eta = 0$; · · · · ·, $\eta = -0.5$; —·—, $\eta = -1.0$.

Vertical profiles of the pressure, together with x- and z-velocity components inside the seabed during the third period are plotted in figure 5. The vertical profiles are similar to those of sinusoidal waves, except that they are not symmetric under cnoidal waves.

3.2.3. *Solitary wave*

Under a solitary wave, the dimensionless dynamic pressure along the water–seabed interface can be calculated as

$$p_b = \operatorname{sech}^2\left[\sqrt{\frac{3\epsilon}{4\mu^2}}\xi\right], \tag{3.20}$$

where

$$\xi = x - Ct, \quad C = \sqrt{1+\epsilon}, \quad \mu = \frac{h'}{L'_x}. \tag{3.21}$$

In the following analysis we select $\epsilon = \mu^2 = 0.2$ as an example. Time histories of p, u, and w at three different elevations, $\eta = 0$, -0.5, and -1.0, respectively are presented in figure 6. Figure 7 shows the vertical profiles of these quantities at several phases. It is interesting to observe that under a solitary wave, water particles above the seabed always move in the same direction as that of wave propagation. However, the horizontal component of the seepage velocity reverses its direction when the horizontal pressure gradient changes its sign. The corresponding vertical component of the seepage velocity also changes direction from negative (downward) to positive (upward).

https://doi.org/10.1017/S0022112007007057 Published online by Cambridge University Press

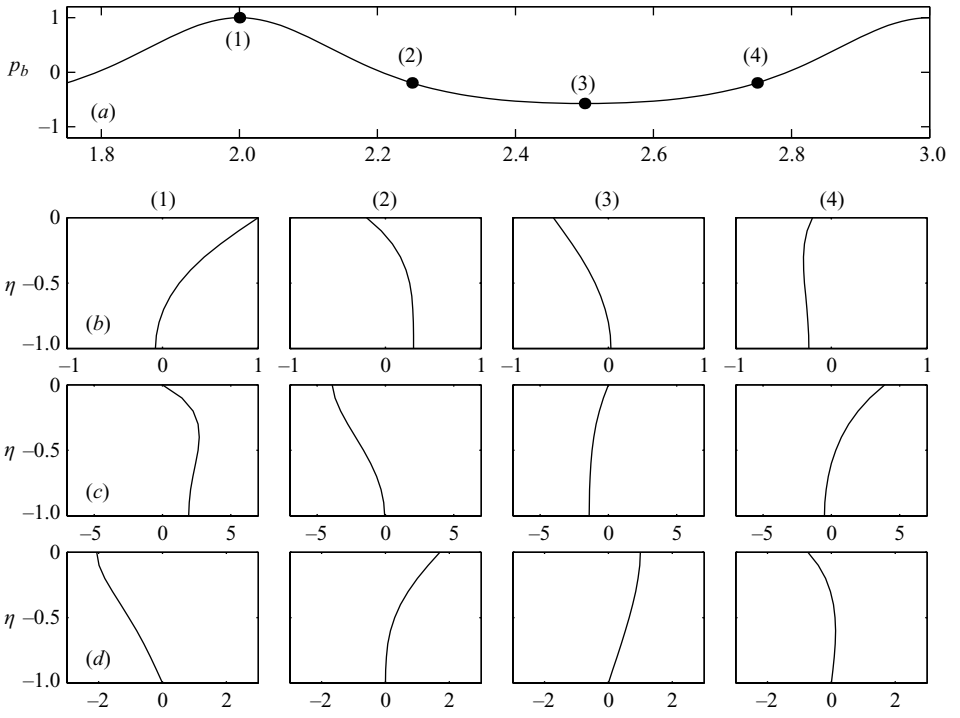


FIGURE 5. Vertical profiles of dimensionless dynamic pressure, p (b), dimensionless horizontal seepage velocity, u (c), and dimensionless vertical seepage velocity, w (d), in a seabed under a cnoidal wavetrain. (a) The time history of the dimensionless dynamic pressure at the water–seabed interface, p_b. The vertical profiles are plotted at four different phases as indicated by numbers in brackets, corresponding to four columns.

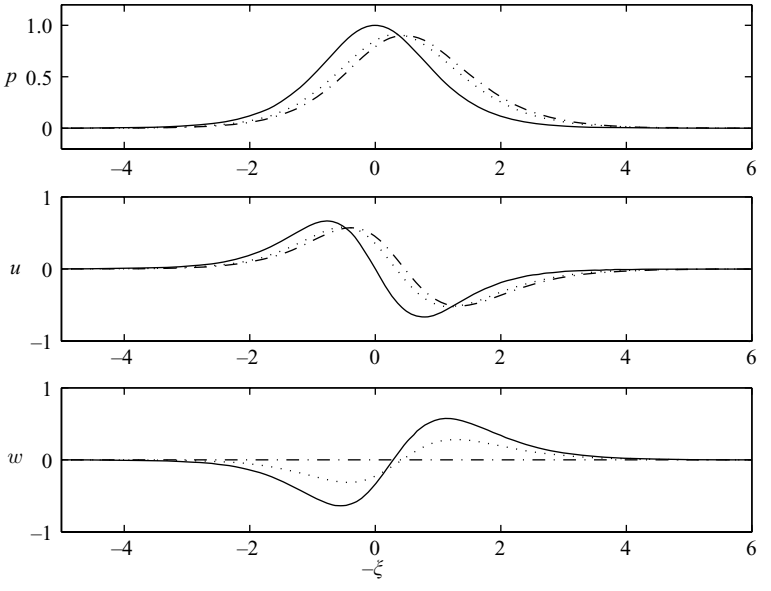


FIGURE 6. Time histories of dimensionless dynamic pressure, p, dimensionless horizontal seepage velocity, u, and dimensionless vertical seepage velocity, w, in a seabed under a solitary wave at three different vertical locations inside the seabed: ——, $\eta = 0$; · · · · ·, $\eta = -0.5$; —•—, $\eta = -1.0$.

https://doi.org/10.1017/S0022112007007057 Published online by Cambridge University Press

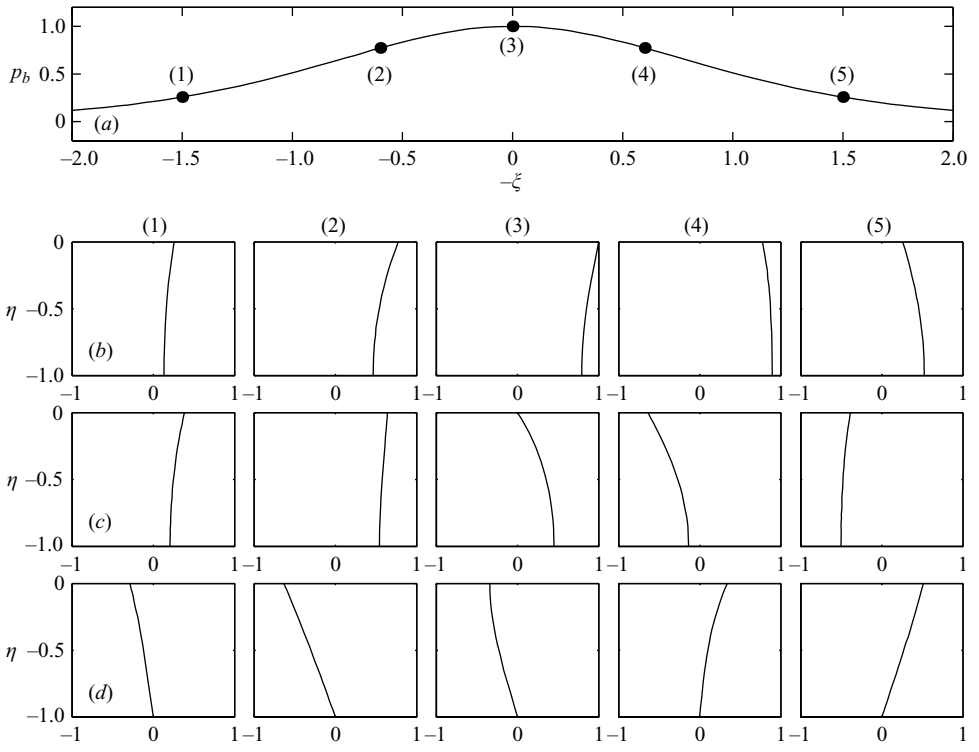


FIGURE 7. Vertical profiles of dimensionless dynamic pressure, p (b), dimensionless horizontal seepage velocity, u (c), and dimensionless vertical seepage velocity, w (d), in a seabed under a solitary wave. (a) The time history of the dimensionless dynamic pressure at the water–seabed interface, p_b. The vertical profiles are plotted at five different phases as indicated by numbers, corresponding to five columns.

3.2.4. *Bore*

Packwood & Peregrine (1980) suggested the following water–seabed interface pressure distribution under a bore:

$$p_b = \frac{1}{2}\left\{1 - \tanh\left[\sqrt{\frac{3\epsilon}{4\mu^2}}\,(x - Vt)\right]\right\}, \tag{3.22}$$

where V is the bore velocity. Using this model pressure distribution along the water–seabed interface, the pore-water pressure and the seepage velocity components inside the seabed are calculated (see figure 8 and figure 9), setting $\epsilon = \mu^2 = 0.2$. As can be seen in these figures, p_b gradually increases from zero to the maximum value and then maintains the maximum value. Figure 9 shows the vertical profiles of these quantities at several phases. While the time history of the horizontal seepage velocity looks like an elevated (positive) soliton, the vertical component looks like a depression (negative) soliton. The peaks of these solitons are shifted from one elevation to another and the diffusion processes are clearly observed in these figures.

4. Direct numerical simulations

The analytical solutions given by (3.8) are limited to the physical condition in which the vertical length scale, either the thickness of the seabed or the diffusion length scale,

https://doi.org/10.1017/S0022112007007057 Published online by Cambridge University Press

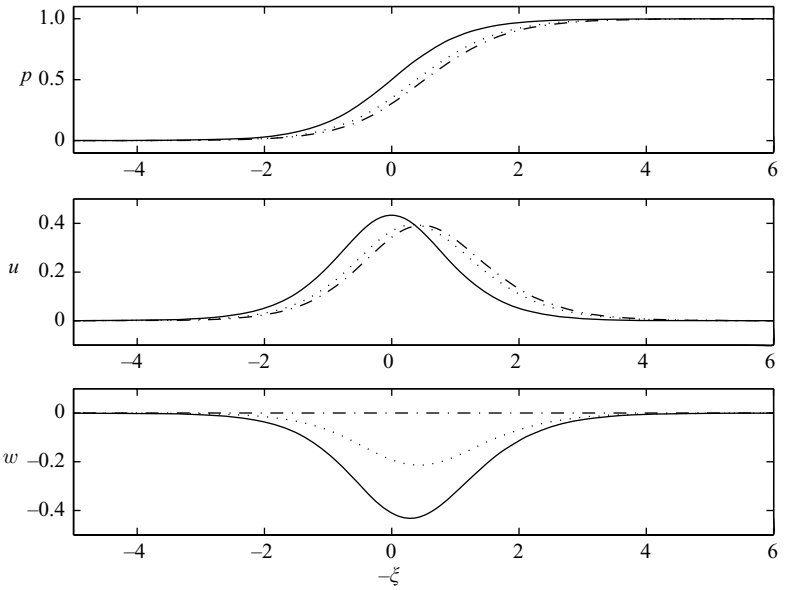


FIGURE 8. Time histories of dimensionless dynamic pressure, p, dimensionless horizontal seepage velocity, u, and dimensionless vertical seepage velocity, w, in a seabed under a bore at three different vertical locations inside the seabed: ——, $\eta = 0$; · · · · ·, $\eta = -0.5$; —·—, $\eta = -1.0$.

is much smaller than the horizontal length scale (i.e. wavelength). Furthermore, the effects of the seepage flows on wave motions are ignored. In this section we present direct numerical simulations without the approximations adopted in the analytical solutions. The direct numerical simulations are based on a two-dimensional Navier–Stokes equation solver with the capability of tracking free-surface movements with a volume of fluid (VOF) method (Lin & Liu 1998). The Navier–Stokes equation solver is coupled with the governing equation for the seepage flows in the seabed, (2.2). The continuity of velocity components and pressure constitutes the necessary boundary conditions coupling wave motions and flows in the seabed. Therefore, solutions obtained from the direct numerical simulations contain the influence of the seabed on wave propagation.

The two-step projection method (Chorin 1968) is used in the Navier–Stokes equation solver and during the second step the intermediate velocity field (u'^*, w'^*) is projected onto a divergence-free plane to obtain the Poisson pressure equation (PPE) as (in the dimensional form)

$$\frac{\partial}{\partial x'}\left(\frac{1}{\rho'^n}\frac{\partial p'^{n+1}}{\partial x'}\right)+\frac{\partial}{\partial z'}\left(\frac{1}{\rho'^n}\frac{\partial p'^{n+1}}{\partial z'}\right)=\frac{1}{\Delta t'}\left(\frac{\partial u'^*}{\partial x'}+\frac{\partial w'^*}{\partial z'}\right), \tag{4.1}$$

in which the superscript $n+1$ denotes the $(n+1)$th time step. The governing equation for the flows in the seabed, (2.2), can be cast in a similar way (in the dimensional form):

$$\frac{\partial}{\partial x'}\left(\frac{1}{\rho'^n}\frac{\partial p'^{n+1}}{\partial x'}\right)+\frac{\partial}{\partial z'}\left(\frac{1}{\rho'^n}\frac{\partial p'^{n+1}}{\partial z'}\right)-\frac{ng'}{k'\overline{K}'_w\Delta t'}p'^{n+1}=\frac{ng'}{k'\overline{K}'_w\Delta t'}p'^n, \tag{4.2}$$

in which $\Delta t'$ is the time step size. Equations (4.1) and (4.2) are solved simultaneously with the requirement that the pressure field is continuous across the water–seabed

https://doi.org/10.1017/S0022112007007057 Published online by Cambridge University Press

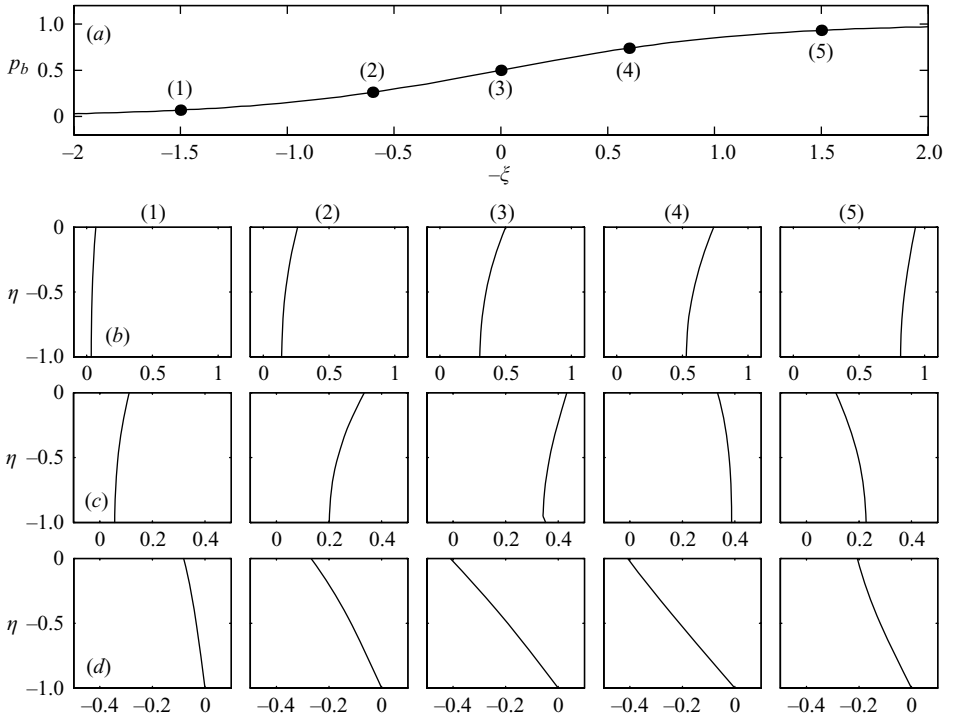


FIGURE 9. Vertical profiles of dimensionless dynamic pressure, p (b), dimensionless horizontal seepage velocity, u (c), and dimensionless vertical seepage velocity, w (d), in a seabed under a bore. (a) The time history of the dimensionless dynamic pressure at the water–seabed interface, p_b. The vertical profiles are plotted at five different phases as indicated by numbers, corresponding to five columns.

interface. Once the pressure field is calculated, the flow velocity inside the seabed can be calculated directly from Darcy's law, (2.1). Detailed descriptions of the VOF method and the implementations of boundary conditions with the two-step projection method can be found in Lin & Liu (1998) and Lin (1998).

4.1. *Numerical set-up*

Numerical results to be presented in the following sections are based on direct numerical simulations in a numerical wave flume which is 20 m long with a water depth of 0.5 m. A numerical wavemaker is installed at the left-hand end of the flume and the first 2 m of the flume has a rigid bottom so that the wavemaker movements do not interact with the seabed directly. A seabed with prescribed properties is placed in the rest of the flume. A sponge layer is installed near the end of the the numerical wave flume to absorb the outgoing waves. The length of the sponge layer is adjustable for the best efficiency of wave dissipation. In all simulations, the numerical wave reflection from the end of the computational domain is typically less than 5 % of the incident wave. Uniform rectangular grids (2 cm $\times$ 1 cm) are used. Solitary waves with 0.1 m wave height are generated using Goring's theory (Goring 1978). To be consistent with the example given in § 3.2.3, we have fixed $\epsilon = \mu^2 = 0.2$.

4.2. *Numerical results for* $D_z \gg D_x$

In the development of our theoretical solution, we have assumed that the horizontal length scale (L'_x) is much larger than the vertical length scale (L'_z), so that the

https://doi.org/10.1017/S0022112007007057 Published online by Cambridge University Press

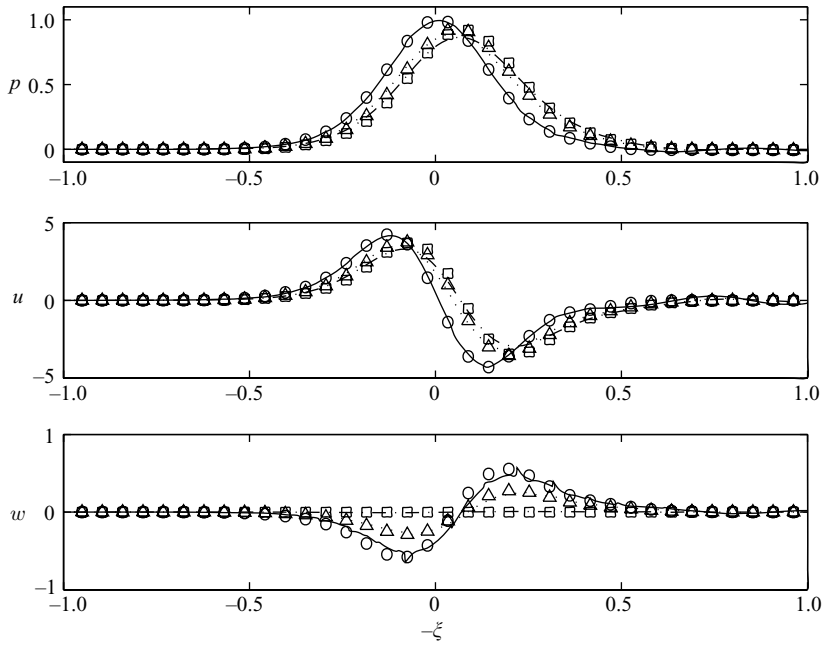


FIGURE 10. Time histories of dimensionless dynamic pressure, p, dimensionless horizontal seepage velocity, u, and dimensionless vertical seepage velocity, w, in a seabed under a solitary wave at three different vertical locations inside the seabed obtained from two-dimensional DNS solutions and one-dimensional analytical solutions, respectively, for $D_z \gg D_x$: ——, DNS data at $\eta = 0$; · · · · ·, DNS data at $\eta = -0.19$; —·—, DNS data at $\eta = -0.38$; ○, analytical solution at $\eta = 0$; △, analytical solution at $\eta = -0.19$; □, analytical solution at $\eta = -0.38$.

governing equation can be approximated as a one-dimensional problem, i.e. $D_z \gg D_x$. In this section, we obtain DNS results for this situation. The thickness of the seabed, d', is assumed to be the same as the water depth, i.e. $d' = 0.5$ m. By choosing the thickness of the seabed as the vertical length scale, D_x and D_z are calculated as 0.03 and 7.03, respectively. Thus, $D_z \gg D_x$ is an adequate assumption.

To compare the results from the analytical solution and the DNS, the dynamic pressure at the water–seabed interface obtained from the DNS is used as the forcing for the theoretical solution. The dynamic pressure at the interface is curve-fitted using the sum of five Gaussian functions:

$$p_b(\xi) = \sum_{i=1}^{5} a_i \exp\left[(\xi - b_i)^2 / c_i^2\right], \tag{4.3}$$

where, $\xi = x - Ct$ is a moving coordinate as defined earlier, and a_i, b_i, and c_i are parameters for the curve-fitting. The R-square value for the fitting is 0.9996.

Figure 10 shows the time histories of dynamic pressure and horizontal and vertical seepage velocity components at the centre of the numerical flume ($x' = 10$ m) at three vertical locations, $z = z'/d' = 0, -0.5, -1.0$. The two different solutions agree fairly well. In the DNS calculation, the solitary wave has travelled a distance of twenty water depths (or about one wavelength) before reaching the mid-section of the flume. The wave-seabed interaction has resulted in minor wave deformation, which can be seen in the time history of dynamic pressure at the water–seabed interface. The vertical profiles of pressure and velocity components evaluated at four wave phases

https://doi.org/10.1017/S0022112007007057 Published online by Cambridge University Press

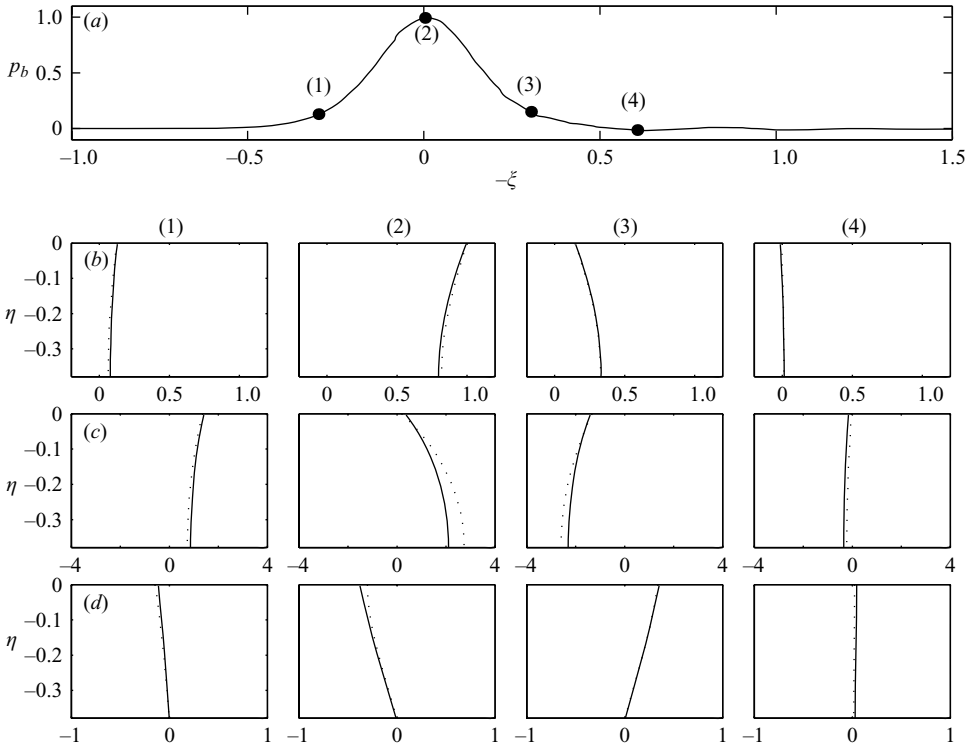


FIGURE 11. Vertical profiles of dimensionless dynamic pressure, p (b), dimensionless horizontal seepage velocity, u (c), and dimensionless vertical seepage velocity, w (d), in a seabed under a solitary wave for $D_z \gg D_x$: ——, two-dimensional DNS solutions; · · · · ·, one-dimensional analytical solution. (a) The time history of the dimensionless dynamic pressure at the water–seabed interface, p_b. The vertical profiles are plotted at four different phases as indicated by numbers, corresponding to four columns.

are presented in figure 11. Overall, good agreement between the solutions is observed. The horizontal velocity, however, shows larger discrepancies, possibly because the slight error in curve-fitting of the dynamic pressure at the water–seabed interface is amplified when the double differentiation is performed in calculating the horizontal velocity, (3.9). Figure 12 shows the contour plot of dimensionless dynamic pressure, p, on $(-\xi)$–η (i.e. time – vertical coordinate) space at a fixed x-location. It is clear that at a given time ($-\xi$ value) the pressure is almost uniform in the entire seabed, i.e. the influence of wave loading has reached the bottom of the seabed almost instantaneously. Thus, the choice of the vertical length scale is justified.

4.3. *Numerical results for* $D_z \approx D_x$

In this section, we increase the thickness of the seabed by the factor of 10, i.e. $d' = 5$ m. Other parameters are identical to those used in the previous section. D_x and D_z are calculated as 0.03 and 0.07, respectively if the thickness of the seabed is used as the vertical length scale. Clearly, since $D_z \approx D_x$ the assumption for the analytical solution is not satisfied in this case. However, very good agreement between the analytical solutions and DNS results can be seen in figures 13 and 14 for the time histories and vertical profiles of pressure and velocity components in the seabed. This is not surprising. Since the wave period of the solitary wave is roughly 3.5 s, the diffusion

https://doi.org/10.1017/S0022112007007057 Published online by Cambridge University Press

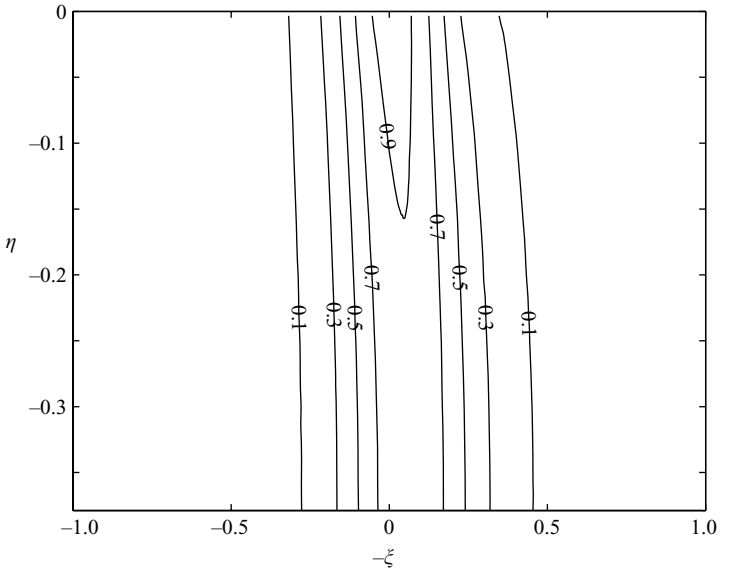


FIGURE 12. Contours of dimensionless dynamic pressure, p, under a solitary wave for $D_z \gg D_x$, on $(-\xi)$–η (i.e. time – vertical coordinate) space at a fixed x-location.

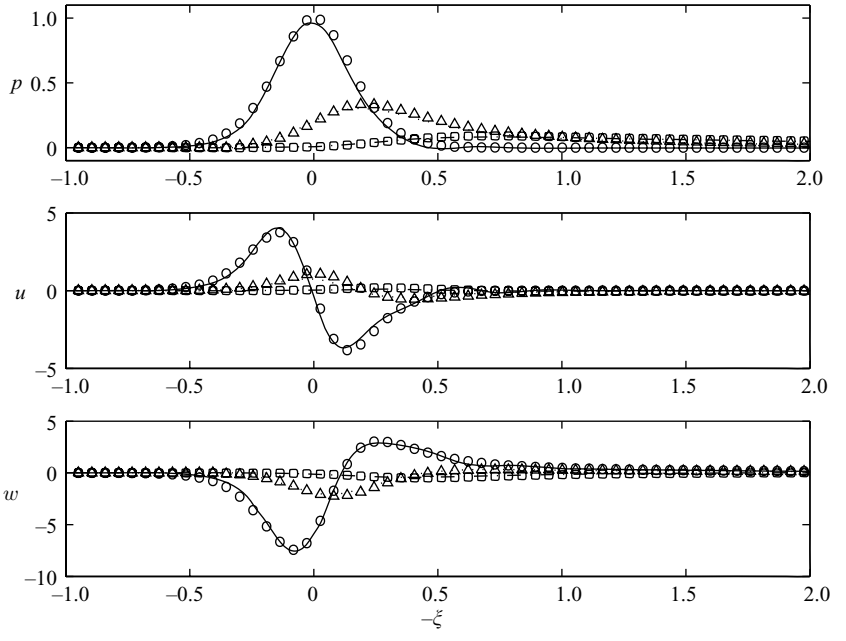


FIGURE 13. Time histories of dimensionless dynamic pressure, p, dimensionless horizontal seepage velocity, u, and dimensionless vertical seepage velocity, w, in a seabed under a solitary wave at three different vertical locations inside the seabed obtained from two-dimensional DNS solutions and one-dimensional analytical solutions, respectively, for $D_z \approx D_x$: ——, DNS data at $\eta = 0$; · · · · ·, DNS data at $\eta = -1.89$; —·—, DNS data at $\eta = -3.78$; ○, analytical solution at $\eta = 0$; △, analytical solution at $\eta = -1.89$; □, analytical solution at $\eta = -3.78$.

https://doi.org/10.1017/S0022112007007057 Published online by Cambridge University Press

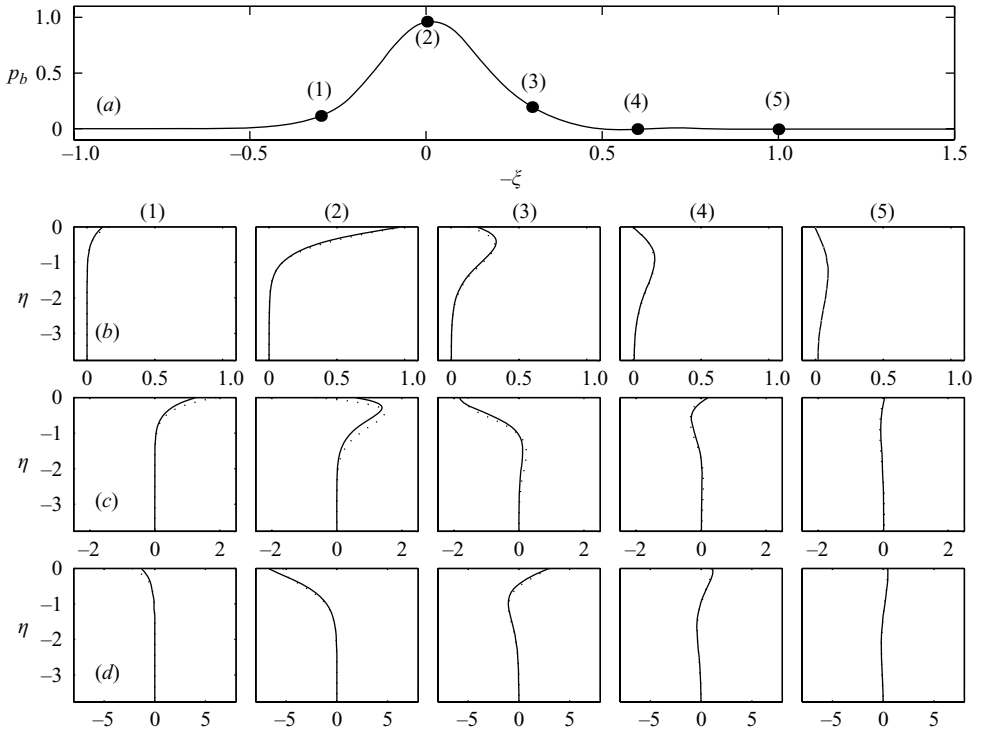


FIGURE 14. Vertical profiles of dimensionless dynamic pressure, p (b), dimensionless horizontal seepage velocity, u (c), and dimensionless vertical seepage velocity, w (d), in a seabed under a solitary wave for $D_z \approx D_x$: ——, two-dimensional DNS solutions; · · · · ·, one-dimensional analytical solutions. (a) The time history of the dimensionless dynamic pressure at the water–seabed interface, p_b. The vertical profiles are plotted at five different phases as indicated by numbers, corresponding to five columns.

length scale can be calculated from (3.3) as 1.4 m, which is much smaller than the thickness of the seabed. This is illustrated in figure 15.

5. Discussion

5.1. *Liquefaction potential inside the seabed*

Momentary liquefaction could occur when the vertical or the horizontal pressure gradient exceeds a certain value. For example, Bear (1972) argued that the porous bed can be momentarily and locally fluidized if the vertical net force on a granular particle is zero. This implies that in terms of dimensional variables:

$$\frac{w'}{k'} > \frac{\gamma_s'}{\gamma_f'}, \tag{5.1}$$

in which γ_s' is the submerged specific weight of the particle and $\gamma_f' = \rho' g'$ the specific weight of water. In terms of the dimensionless variables employed in this paper, the liquefaction criterion becomes

$$-\frac{\partial p}{\partial \eta} \geqslant \frac{\gamma_s'}{\gamma_f'} \frac{L_z' \sqrt{D_z}}{a'}, \tag{5.2}$$

https://doi.org/10.1017/S0022112007007057 Published online by Cambridge University Press

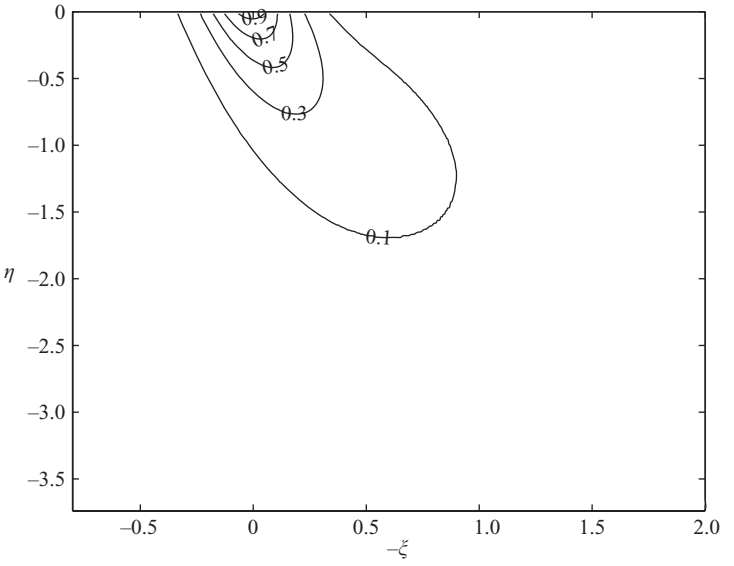


FIGURE 15. Contours of dimensionless dynamic pressure, p, under a solitary wave for $D_z \approx D_x$, on $(-\xi)-\eta$ (i.e. time − vertical coordinate) space at a fixed x-location.

which can be further reduced to

$$-\frac{\partial p}{\partial \eta} \geqslant \frac{\gamma_s'}{\gamma_f'} \frac{L_x' \sqrt{D_x}}{a'} = \frac{\gamma_s'}{\gamma_f'} \frac{L_x'/h'}{\epsilon} \sqrt{D_x}, \tag{5.3}$$

where L_x'/h' is either given in (3.18) for the cnoidal wave, or specified as $1/\mu$ for the solitary wave and the bore, while D_x is given in (2.5). It is clear that the momentary liquefaction can occur more easily for smaller values of D_x, which corresponds to a lower degree of saturation in the seabed.

On the other hand, Madsen (1974) suggested that the momentary liquefaction can also occur if the pore-water pressure gradient in the horizontal direction exceeds the intergranular stress. After making several simplifying assumptions, Madsen (1974) presented the following criterion:

$$\left|\frac{\partial p}{\partial x}\right| \geqslant \frac{\gamma_s'}{\gamma_f'} \tan\theta \frac{L_x'/h'}{\epsilon}, \tag{5.4}$$

where θ is the internal friction angle.

As an example, we consider a wavetrain in a coastal region of 10 m water depth, which can be described as a cnoidal wave with $\epsilon = 0.2$ and $m = 0.6$. The corresponding wavelength and the wave period can be calculated as $L_x' = 78$ m and $T' = 8.8$ s, respectively. The seabed of thickness $d' = 10$ m is made of relatively loose sand with hydraulic conductivity $k' = 10^{-4}$ m s^{-1}, porosity $n = 0.3$, and the degree of saturation $S_r = 0.995$. The effective bulk modulus of elasticity can be calculated as $\overline{K}_w' = 2 \times 10^7$ N m^{-2}. We further assume that $\gamma_s' \tan\theta/\gamma_f' = 0.5$. Thus, the critical pressure gradients in both directions, (5.3) and (5.4), are determined as 2.46 in the vertical direction and 14.54 in the horizontal direction, respectively. Using the theoretical solutions, (3.9) and (3.10), the maximum pore-water pressure gradients along the water–seabed interface under the specified wave conditions are 2.02 and 5.98 in the vertical and the horizontal directions, respectively. Thus, under the present

https://doi.org/10.1017/S0022112007007057 Published online by Cambridge University Press

wave conditions and seabed properties, the vertical as well as the horizontal pore-water velocities are not strong enough to cause momentary liquefaction. We reiterate here that this analysis is sensitive to the degree of saturation. That is, if S_r is changed to 0.990, the effective bulk modulus of elasticity of the fluid, $\overline{K}'_w$, decreases by half ($1 \times 10^7\,\mathrm{N\,m^{-2}}$), and the critical vertical pressure gradient decreases to 1.73, which is now smaller than the maximum vertical pore-water pressure gradient. Consequently, the momentary liquefaction can occur.

5.2. *Wave damping rate*

Packwood & Peregrine (1980) argued that the energy dissipation rate inside the seabed can be calculated by integrating the pressure work done along the water–seabed interface. Scaling the energy dissipation rate as

$$\frac{1}{2}\rho' g' a_o'^2 \frac{L'_x}{T'},$$

the dimensionless energy dissipation rate can be calculated from

$$D = 2a^2 k' \frac{T'}{L'_x}\frac{L'_x}{L'_z}\int_\Gamma pw\,|_{\eta=0}\,\mathrm{d}x, \tag{5.5}$$

where the local dimensionless wave amplitude, a, has been scaled by the initial (or undamped) wave amplitude a'_o and the integration on the right-hand side is integrated over Γ, which is the effective wavelength for the periodic waves and solitary waves. Given the expression for the total wave energy within one wavelength, E'_t, which can be normalized by

$$\frac{1}{2}\rho' g' a_o'^2 L'_x,$$

the dimensionless wave damping rate can be found from the following relationship:

$$D = \mathrm{d}E_t/\mathrm{d}t. \tag{5.6}$$

Up to the first order of accuracy, the dimensionless wave energy in a wavelength per unit width can be expressed as follows:

$$E_t = a^2 \tag{5.7}$$

for the sinusoidal wave,

$$E_t = 2H^2 f(m), \tag{5.8}$$

where

$$f(m) = \frac{1}{3m^2}\left\{2(2-m)\frac{E}{K} - 3\frac{E^2}{K^2} - (1-m)\right\}, \tag{5.9}$$

for the cnoidal wave (Miles 1979), and

$$E_t = \frac{16}{3\sqrt{3}}\frac{\mu}{\epsilon^{1/2}}a^{3/2} \tag{5.10}$$

for the solitary wave (Longuet-Higgins 1974). Note that $f(m)$ becomes 1/8 as m goes to zero, and that (5.8) reduces to (5.7) with $H = 2a$. On the other hand, as m increases to 1, $f(m)$ can be approximated as

$$f(m) \approx \frac{8}{3\sqrt{3}}\frac{\mu}{\sqrt{H}\epsilon^{1/2}}; \tag{5.11}$$

https://doi.org/10.1017/S0022112007007057 Published online by Cambridge University Press

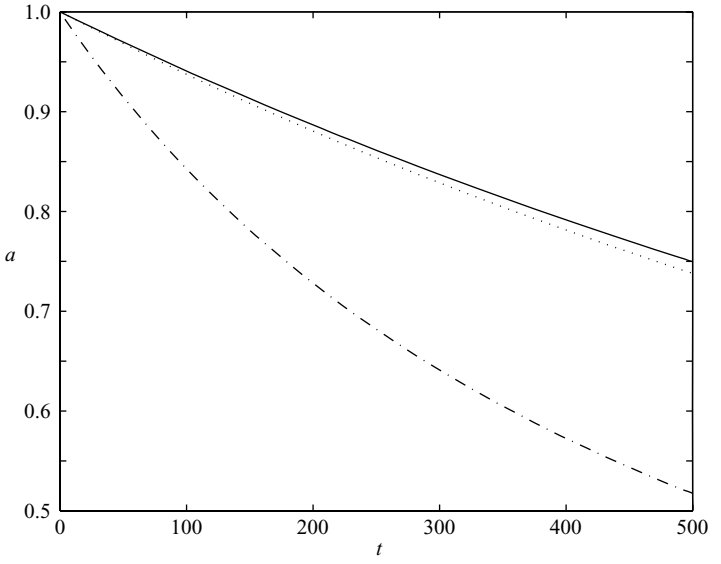


FIGURE 16. The wave amplitude attenuation of a solitary wave due to the seepage flows in a shallow seabed: ——, $S_r = 0.990$ and · · · · ·, $S_r = 0.995$ calculated from (5.15); —·—, $S_r = 1.000$ calculated from the expression by Packwood & Peregrine (1980).

thus, (5.8) becomes (5.10) with $H = a$. To be consistent with the other cases, (5.8) can be rewritten in terms of the wave amplitude (a, the maximum positive water-surface displacement):

$$E_t = \frac{2}{3}\left[\frac{2(2-m)EK - 3E^2 - (1-m)K^2}{(K-E)^2}\right] a^2. \tag{5.12}$$

By substituting (5.7), (5.10), and (5.12) into (5.6), respectively, we can obtain expressions for the rate of wave amplitude changes in the following dimensionless forms:

$$\frac{\mathrm{d}a}{\mathrm{d}t} = a\left(\frac{k'T'}{L'_z}\int_\Gamma pw\,|_{\eta=0}\,\mathrm{d}x\right) \tag{5.13}$$

for sinusoidal waves,

$$\frac{\mathrm{d}a}{\mathrm{d}t} = a\left[\frac{k'T'}{L'_z}\frac{3(K-E)^2}{2\{2(2-m)EK - 3E^2 - (1-m)K^2\}}\int_\Gamma pw\,|_{\eta=0}\,\mathrm{d}x\right] \tag{5.14}$$

for cnoidal waves, and

$$\frac{\mathrm{d}a}{\mathrm{d}t} = \frac{\epsilon^{1/2}}{\mu}a^{3/2}\left(\frac{\sqrt{3}}{4}\frac{k'T'}{L'_z}\int_\Gamma pw\,|_{\eta=0}\,\mathrm{d}x\right) \tag{5.15}$$

for a solitary wave. Note that (5.13), (5.14), and (5.15) are nonlinear differential-integral equations for the dimensionless wave amplitude and must be solved numerically.

As an example, we examine here the damping rate of a solitary wave with initial wave amplitude $a'_o = 0.04\,\mathrm{m}$ in a water depth $h' = 0.1\,\mathrm{m}$ ($\epsilon = 0.4$) over a permeable seabed of thickness $d' = 0.1\,\mathrm{m}$ ($L'_z = d'$). The seabed is composed of coarse sand ($k' = 10^{-2}\,\mathrm{m\,s^{-1}}$) with porosity $n = 0.3$. The effective wavelength $L'_x = 1.09\,\mathrm{m}$ is defined as the distance within which 99 % of the surface elevation of the solitary wave is

https://doi.org/10.1017/S0022112007007057 Published online by Cambridge University Press

included. Thus $\mu = 0.089$ and the corresponding effective wave period is $T' = 0.93$ s. Euler's method with the time step $\Delta t' = 1$ s is used to solve (5.15). The results are presented in figure 16 for three different degrees of saturation, where the results for saturated flows are taken from the expression suggested by Packwood & Peregrine (1980). The wave damping rate is smaller for the unsaturated cases. For the saturated flow, the entire flow field responds instantaneously to the wave loading at the water–seabed interface. On the other hand for the unsaturated flows, only a portion of the seabed is affected. Consequently, a smaller amount of pressure work is required and leads to a smaller wave damping rate in the unsaturated flow case.

6. Concluding remarks

In this paper we have presented an approximate analytical solution for the seepage flows induced by an arbitrary wave field above the permeable seabed, which is assumed to be partially saturated. The analytical solutions require the condition that the horizontal length scale is much greater than the vertical length scale, which can be satisfied when the wavelength of the wave field is much longer than the thickness of the seabed or, in the case of a transient wave event, the vertical diffusion scale. The hypotheses are confirmed by the DNS.

The analytical solutions are used to examine the liquefaction potential under various wave conditions. With the limited understanding of the criterion for momentary liquefaction, we still can conclude that the potential for liquefaction is much higher for the unsaturated flows. Formulae for estimating damping rate for different wave types are also presented. Numerical example shows that flows with higher degree of saturation induce higher wave damping. When the seabed is made of fine sand, the impact of the seabed on wave propagation is small and slow. If the seabed is made of coarse sand or shingle, the impact might increase and the interaction between wave motions and seepage flows might become significant. For future work, a set of Boussinesq-type equations with effects of seepage flows could be derived in a similar approach to that employed by Liu & Orfila (2004).

The authors would like to dedicate this paper to Professor Howell Peregrine who passed away on March 20, 2007.

This research has been supported by grants from the National Science Foundation (Fluid Dynamics Program, Physical Oceanography Program and ITR Program) and from the Office of Naval Research (Geoscience Program) to Cornell University. Yong Sung Park would also like to acknowledge the support from Korea Science and Engineering Foundation under grant number M06-2004-000-10541.

REFERENCES

Bear, J. 1972 *Dynamics of Fluids in Porous Media*. Dover.

Chorin, A. J. 1968 Numerical solution of the Navier-Stokes equations. *Math. Comput*. **22**, 745–762.

Dalrymple, R. A. & Liu, P. L.-F. 1978 Waves over soft muds: a two-layer fluid model. *J. Phys. Oceanogr*. **8**, 1121–1131.

Goring, D. K. 1978 Tsunamis – the propagation of long waves onto a shelf. *Rep*. KH-R-9. W. M. Keck Laboratory of Hydraulics and Water Resources, California Institute of Technology.

Jeng, D. S. 2003 Wave-induced sea floor dynamics. *Appl. Mech. Rev*. **56**, 407–429.

Lin, P. 1998 *Numerical modeling of breaking waves*. PhD Thesis, Cornell University.

Lin, P. & Liu, P. L.-F. 1998 A numerical study of breaking waves in the surf zone. *J. Fluid Mech*., **359**, 239–264.

https://doi.org/10.1017/S0022112007007057 Published online by Cambridge University Press

Liu, P. L.-F. 1973 Damping of water waves over porous bed. *J. Hydraul. Div. ASCE* **99**, 2263–2271.

Liu, P. L.-F. & Chan, I.-C. 2007*a* A note on the effects of a thin visco-elastic mud layer on small amplitude water wave propagation. *Coastal Engng* **54**, 233–247.

Liu, P. L.-F. & Chan, I.-C. 2007*b* On long wave propagation over a fluid-mud seabed. *J. Fluid Mech.* **579**, 467–480.

Liu, P. L.-F. & Orfila, A. 2004 Viscous effects on transient long wave propagation. *J. Fluid Mech.* **520**, 83–92.

Longuet-Higgins, M. S. 1974 On the mass, momentum, energy and circulation of a solitary wave. *Proc. R. Soc. Lond.* A **337**, 1–13.

Macpherson, H. 1980 The attenuation of water waves over a non-rigid bed. *J. Fluid Mech.* **97**, 721–742.

Madsen, O. S. 1974 Stability of a sand bed under breaking waves. In *Proc. 14th Conf. Coastal Engng*, vol. 2, pp. 776–794.

Mei, C. C. 1983 *The Applied Dynamics of Ocean Surface Waves.* John Wiley & Sons.

Mei, C. C. & Liu, P. L.-F. 1993 Surface waves and coastal dynamics. *Annu. Rev. Fluid Mech.* **25**, 215–240.

Miles, J. W. 1979 On the Korteweg-de Vries equation for a gradually varying channel. *J. Fluid Mech.* **91**, 181–190.

Moshagen, H. & Torum, A. 1975 Wave induced pressures in permeable seabeds. *J. Waterways, Harbor, and Coastal Engng. Div. ASCE*, 49–57.

Oumeraci, H. & Kudella, M. 2004 Large scale experiments on a caisson breakwater. *Tech. Rep.* Technical Univ. of Braunschweig, Leichtweiss-Institute.

Packwood, A. R. & Peregrine, D. H. 1980 The propagation of solitary waves and bores over a porous bed. *Coastal Engng* **3**, 221–242.

Sumer, B. M. & Fredsoe, J. 2002 *The Mechanics of Scour in the Marine Environment*. World Scientific.

Wen, J. & Liu, P. L.-F. 1998 Effects of seafloor conditions on water wave damping. In *Advances in Fluid Mechanics: Free Surface Flows and Viscosity* (ed. P. A. Tyrand), vol. 16, pp. 145–178.

Yamamoto, T., Koning, H. L., Sellmeijer, H. & van Hijum, E. 1978 On the response of a poro-elastic bed to water waves. *J. Fluid Mech.* **87**, 193–206.

https://doi.org/10.1017/S0022112007007057 Published online by Cambridge University Press